


Proton MR Spectroscopy of Lesion Evolution in Multiple Sclerosis: Steady-State Metabolism and its Relationship to Conventional Imaging

Ivan I. Kirov ^{1,2*}, Shu Liu,^{1,2} Assaf Tal,³ William E. Wu,^{1,2}
Matthew S. Davitz,^{1,2} James S. Babb,^{1,2} Henry Rusinek,^{1,2}
Joseph Herbert,⁴ and Oded Gonen^{1,2}

¹Center for Advanced Imaging Innovation and Research (CAI²R), New York University School of Medicine, New York, New York

²Bernard and Irene Schwartz Center for Biomedical Imaging, Department of Radiology, New York University School of Medicine, New York, New York

³Department of Chemical Physics, Weizmann Institute of Science, Rehovot, Israel

⁴Multiple Sclerosis Comprehensive Care Center, New York University Langone Medical Center, New York, New York



Abstract: Although MRI assessment of white matter lesions is essential for the clinical management of multiple sclerosis, the processes leading to the formation of lesions and underlying their subsequent MRI appearance are incompletely understood. We used proton MR spectroscopy to study the evolution of *N*-acetyl-aspartate (NAA), creatine (Cr), choline (Cho), and *myo*-inositol (mI) in pre-lesional tissue, persistent and transient new lesions, as well as in chronic lesions, and related the results to quantitative MRI measures of T1-hypointensity and T2-volume. Within 10 patients with relapsing-remitting course, there were 180 regions-of-interest consisting of up to seven semi-annual follow-ups of normal-appearing white matter (NAWM, $n = 10$), pre-lesional tissue giving rise to acute lesions which resolved ($n = 3$) or persisted ($n = 3$), and of moderately ($n = 9$) and severely hypointense ($n = 6$) chronic lesions. Compared with NAWM, pre-lesional tissue had higher Cr and Cho, while compared with lesions, pre-lesional tissue had higher NAA. Resolving acute lesions showed similar NAA levels pre- and post-formation, suggesting no long-term axonal damage. In chronic lesions, there was an increase in mI, suggesting accumulating astrogliosis. Lesion volume was a better predictor of axonal health than T1-hypointensity, with lesions larger than 1.5 cm³ uniformly exhibiting very low (<4.5 millimolar) NAA concentrations. A positive correlation between longitudinal changes in Cho and in lesion volume in moderately hypointense lesions implied that lesion size is mediated by chronic inflammation. These and other results are integrated in a discussion on the steady-state metabolism of lesion evolution in multiple sclerosis, viewed in the context of conventional MRI measures. *Hum Brain Mapp* 00:000–000, 2017. © 2017 Wiley Periodicals, Inc.

Contract grant sponsor: National Institutes of Health award; Contract grant numbers: R01NS097494, R01NS050520, R01NS29029 (National Institute of Neurological Disorders and Stroke) and P41EB017183, R01EB001015 (National Institute of Biomedical Imaging and Bioengineering).

*Correspondence to: Ivan Kirov, Ph.D., Department of Radiology, New York University School of Medicine, 660 First Avenue, 421, New York, New York 10016. E-mail: ivan.kirov@nyumc.org

Received for publication 1 September 2016; Revised 17 April 2017; Accepted 1 May 2017.

DOI: 10.1002/hbm.23647

Published online 00 Month 2017 in Wiley Online Library (wileyonlinelibrary.com).

Key words: proton magnetic resonance spectroscopy; magnetic resonance imaging; white matter; plaques; T1-hypointensity

INTRODUCTION

Multiple sclerosis (MS) lesions are focal, myelin-poor regions with gliosis and reduced axonal density [Frohman et al., 2006]. They arise from autoimmune-mediated inflammation episodes which are directly responsible for patients' overt symptoms and relapses. Over time lesions cause axonal degeneration and cell death [Trapp et al., 1999], which underlie the progressive disability characteristic of advancing disease.

Lesions are the radiological hallmark of MS. They are identified as regions of white matter hyperintensities on T2-weighted MRI, which reflect a wide range of inflammation-induced injury. Specificity to lesion status is possible with T1-weighted imaging: gadolinium chelate enhancement denotes ongoing blood-brain-barrier breakdown; and hypointensity lasting more than 6 months indicates a more terminal degree of injury compared with isointense lesions and those with transient hypointensity [Filippi et al., 2011]. These classifications, and complementary metrics such as lesion number and volume, are essential for individual patient diagnosis, prognosis and treatment monitoring [Lublin et al., 2014], as well as for assessment of therapy efficacy in clinical trials [Cohen et al., 2012; Sormani and Bruzzi, 2013]. Lesion appearance on T1- and T2-weighted imaging, however, depends solely on differences in the relaxation times of water protons, thus precluding differentiation of inflammation, gliosis, demyelination, remyelination, and neuronal loss, all of which contribute to changes in the MRI contrast ratio between lesions and adjacent tissue. A more direct way to assess the underlying pathophysiology is possible with proton MR spectroscopy (^1H MRS) through quantification of metabolites functionally related to specific processes. For example, *N*-acetyl-aspartate (NAA) concentration reflects neuronal health, number and mitochondrial function; creatine (Cr) levels are linked with energy metabolism and glial proliferation; choline (Cho) with de- and remyelination; *myo*-inositol (mI) with astroglial activation and gliosis [Rovira and Alonso, 2013; Sajja et al., 2009]. Besides lending specificity to the conventional MR metrics, ^1H MRS has the potential to inform about the processes leading to lesion formation and to help in predicting lesion appearance on MRI. Unfortunately, ^1H MRS has lower signal-to-noise ratio compared with MRI, necessitating voxels several orders of magnitude larger (cm^3 versus mm^3). This introduces uncertainty in measuring metabolism in all but the largest lesions, because of voxel inclusion of cerebro-spinal-fluid (CSF) and surrounding normal-appearing tissue. The resulting partial volume errors are affected by lesion location (e.g., neighboring CSF versus gray matter), voxel size and

placement, and confound both cross-sectional and longitudinal assessments. Moreover, metabolic ratios (e.g., NAA/Cr, NAA/Cho, and Cho/Cr) often used instead of absolute quantification, do not take into account differences in metabolite relaxation times and can mask changes occurring in both the numerator and denominator.

In this study, therefore, we use absolute quantification with stringent partial volume correction combined with high spatial resolution ^1H MRS imaging (^1H MRSI). This approach enabled us to study lesions in mildly disabled patients with relapsing-remitting (RR) MS, early in its course, when lesions are typically below the resolution of ^1H MRS. Our goal was to provide a comprehensive assessment of the metabolism associated with lesion evolution from pre-lesional to chronic state, and relate that to quantitative measures of conventional MRI. The design was a three year, semi-annual longitudinal follow-up of pre-lesional tissue, resolving and persisting acute lesions, as well as of chronic lesions. Absolute concentrations of NAA, Cr, Cho, and mI were obtained along with T1-contrast ratios and T2-lesion volumes. Changes of these metrics over time were assessed within acute and chronic lesions and comparisons across lesion stages and across lesions stratified by different T1-hypointensity were performed. The results provide insights into lesion pathogenesis and pathophysiology and reveal the metabolic correlates of conventional imaging measures across all stages of lesion evolution.

MATERIALS AND METHODS

Human Subjects

Eighteen patients, 5 men, 13 women, with RR MS [Poser et al., 1983] within 6 years from diagnosis, were scanned semiannually over 3 years (up to 7 scans each). The inclusion criteria were MS diagnosis, no MRI contraindications, ability to provide informed consent, and no history of alcohol, drug abuse, HIV infection, psychiatric, or other neurological comorbidities. The project was approved by the Institutional Review Board and informed consent explaining the nature of the procedures was obtained from all subjects. The study was carried out in accordance with the Code of Ethics of the World Medical Association.

MR Data Acquisition

The following protocol was done in a 3 T scanner (Trio, Siemens AG, Erlangen, Germany) using a circularly-polarized transmit-receive head coil: (1) sagittal MP-RAGE with $TE/TI/TR = 2.6/800/1,360$ ms, $256 \times 256 \times 160$ mm^3

field-of-view (FOV), 1 mm³ isotropic pixels; (2) custom chemical shift imaging-based automatic shimming [Hu et al., 1995]; (3) 3D ¹H MRSI (see below); (4) axial T2-weighted FLAIR with $TE/TI/TR = 88/2,500/9,000$ ms, $FOV = 256 \times 256$ mm², 512×512 matrix, 30 slices, 3.7 mm thickness; (5) intravenous administration of 0.2 mL/kg gadolinium chelate (Magnevist, Bayer HealthCare, Whippany, NJ); (6) axial post-gadolinium chelate T1-weighted spin-echo: $TE/TR = 4.7/349$ ms, $FOV = 256 \times 256$ mm², 512×512 matrix, 30 slices, 3.5 mm thickness. During the scan, the MP-RAGE images were reformatted into axial orientation at an angle rendering the genu and splenium of the corpus callosum in the same horizontal plane at the level of the longitudinal fissure. All subsequent scans were acquired at the same angle. The pre- and post-gadolinium chelate T1-weighted scans were compared to confirm that the head remained in its initial position at the end of the scan.

The ¹H MRSI volume-of-interest (VOI), with right-left (RL) \times anterior-posterior (AP) \times superior-inferior (SI) dimensions of $8 \times 10 \times 4.5$ cm³, was placed as superior in the brain as possible while avoiding the subcutaneous lipids, as shown in Figure 1A–C. It was excited with $TE/TR = 35/1,800$ ms PRESS (point-resolved spectroscopy) in three 1.5 cm thick, second-order Hadamard-encoded slabs (6 slices) interleaved every TR along the SI direction for optimal signal-to-noise ratio and spatial coverage [Goelman et al., 2006b]. The axial slabs were encoded with 2D 16×16 chemical shift imaging over a 16×16 cm² FOV and a 8×10 cm VOI defined in their planes with two 11.2 ms-long, numerically optimized, 180° radio-frequency pulses (4.5 kHz bandwidths) under 1.34 and 1.1 mT/m gradients, yielding 480 voxels, a nominal 0.75 cm³ each, or approximately $1.2 \times 1.2 \times 0.75 = 1.08$ cm³ given the full-width at half maximum of the point spread function for the uniform 2D phase encoding in the axial planes [Brooker et al., 1987; Goelman et al., 2006a; Mareci and Brooker, 1991]. The MR signal was acquired for 256 ms at ± 1 kHz bandwidth. At two averages, the ¹H MRSI took 34 minutes and the entire protocol about 1.2 hours.

Segmentation

Binary masks of all lesions within the patient cohort were generated on the FLAIR images using locally developed software [Rusinek et al., 2013]. To ensure accurate lesion segmentation, each slice was inspected by an operator who manually modified the masks if needed. Lesion volumes were calculated as the product of the number of “lesion pixels” \times pixel volume. Only lesions larger than 0.3 cm³ were retained for analysis; this was the minimal volume that could result in at least 40% lesion fraction within a single, 0.75 cm³, ¹H MRSI voxel. Pre-lesional tissue was defined as a region in which a lesion satisfying the size criterion appeared at a subsequent timepoint. The MP-RAGE images were segmented into CSF, gray matter (GM), and white matter (WM) masks using SPM2 [Ashburner

and Friston, 1997], as shown in Figure 2. Normal-appearing white matter (NAWM) was obtained by subtracting the lesion and pre-lesional tissue masks from the WM mask. To avoid peri-lesional tissue, prior to the subtraction the lesion and pre-lesional masks were inflated by 3 mm in all directions. In addition, since the pre-lesional mask denoted only future lesions larger than 0.3 cm³, the pre-lesional tissue of any smaller new lesions was also excluded.

Image and Mask Co-Registration

Lesions were segmented from the FLAIR, while tissue and CSF were segmented from the MP-RAGE. To account for the different spatial resolution of the resulting masks, co-registration was performed using FLAIR as the source, MP-RAGE as the target space, and mutual information as the voxel-based similarity measure. The transformation matrix was applied to the lesion mask in order to co-register it to the MP-RAGE space (Fig. 2B). Sub-voxel interpolation assured unbiased target mask. Since hypointense lesions are often mislabeled as tissue or as CSF by segmentation algorithms [Chard et al., 2010], the transformed lesion masks were subtracted from the GM and the CSF masks, eliminating misclassified pixels, as shown in Figure 2C. All masks, now in MP-RAGE space, were co-registered with the ¹H MRSI based on DICOM-stored positioning information, yielding their volume in every ¹H MRSI voxel.

To delineate pre-lesional tissue, FLAIR images from the timepoint at which the lesion first appeared were co-registered (using the rigid-body model and absolute signal difference as the similarity measure) to FLAIR images of the preceding timepoint(s), and the transformation matrix was applied to the lesion mask, creating a “ghost” mask of the forthcoming lesion.

Co-registration accuracy of all procedures was visually verified on multiple slices. Locally developed software was used for all co-registration tasks [Sigmund et al., 2012].

Lesion Characterization

Lesions were classified as chronic if present at the preceding scan (6 month interval definition [Davie et al., 1997]), and as acute (i.e., “new”) if otherwise. For lesions present at the baseline scan, prior MRI scans were consulted to confirm a chronic classification.

Each lesion’s T1-hypointensity was assessed from the MP-RAGE obtained prior to gadolinium chelate administration. Isointense lesions were defined as having signal intensity within 2 standard deviations of adjacent NAWM intensity, while lesions with lower intensity were classified as hypointense. A category of “severely hypointense” lesions was defined as having signal intensity less than 2 standard deviations of adjacent cortical normal-appearing GM (NAGM) intensity. All other hypointense lesions were termed “moderately hypointense.” To enable inter-scan comparison

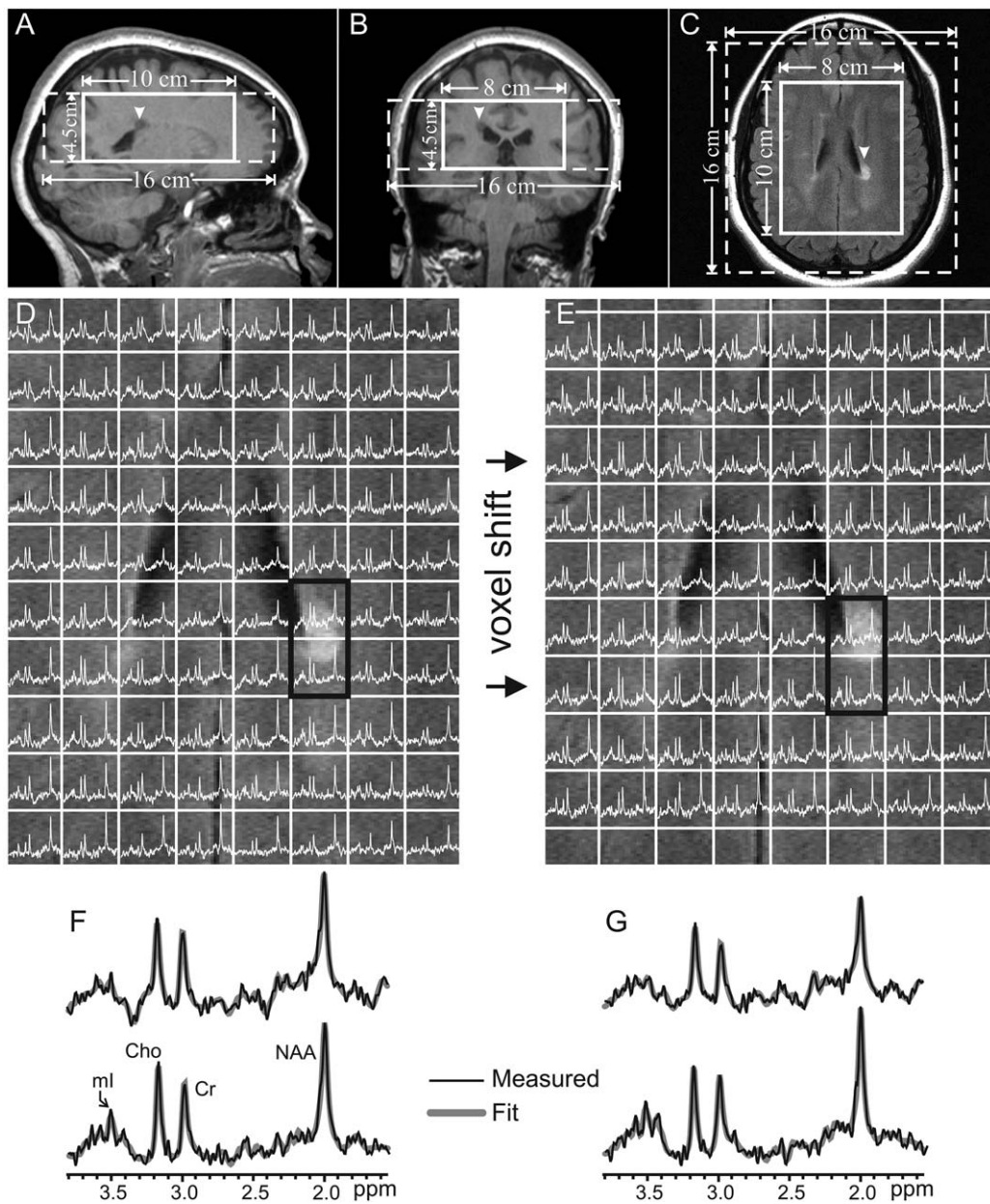


Figure 1.

Positioning of the ¹H MRSI VOI and voxel shifting. Top: Sagittal (A) and coronal (B) T1-weighted MP-RAGE, and axial (C) T2-weighted FLAIR of patient #9 in Table I, superimposed on the volume of interest and field of view (solid and dashed white frames). The location of lesion #18 is indicated on all sections by a white arrowhead. Middle: (D) Real part of the 8 × 10 (left–right × anterior–posterior) ¹H spectra matrix from the spectroscopic slice corresponding to the axial section on (C), overlaid on the magnified anatomy with voxel partitions shown. Note that the lesion of interest is contained within two voxels (thick black lines). (E) The ¹H spectra matrix from (D) after

voxel shifting to minimize partial volume effects from CSF and normal appearing tissue. The parameters were 3 mm (3/10 voxel) along the posterior axis and 1 mm (1/10 voxel) along the right axis. Note that the voxel shifted data would be identical to data *originally* acquired under these new offsets. Bottom: Expanded and magnified spectra from the four voxels delineated with a black outline in (D) and (E), superimposed on their fitted model functions (gray lines). Note the change of spectral appearance before (F) and after (G) voxel shifting, consistent with increasing lesion content within the top voxel and decreasing lesion content in the bottom voxel.

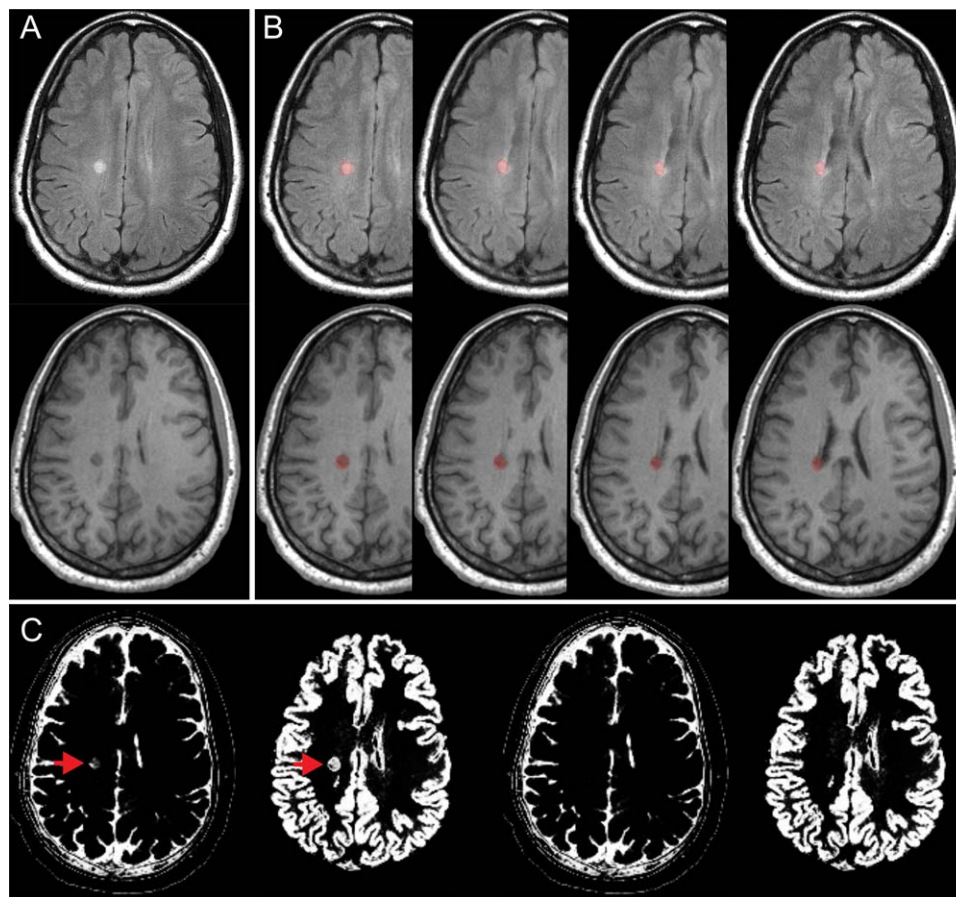


Figure 2.

Segmentation and MRI co-registration. (A) Axial T2-weighted FLAIR (top) and its corresponding T1-weighted MP-RAGE image (bottom), showing the first timepoint of lesion #3 in Table I. (B) The FLAIR (top) is co-registered to the MP-RAGE (bottom) and the transformation matrix is used to co-register the lesion mask to the MP-RAGE. (C) The CSF and GM masks obtained from the MP-RAGE slice shown in (A) show that the

segmentation software can incorrectly register the lesion as CSF and as GM (red arrows). These misregistered pixels were removed by subtracting the lesion mask in (B) from the CSF and GM masks. The resultant masks (lower right) no longer contain misregistration errors, and can be used for calculating CSF and GM partial volumes in the spectroscopic voxels. [Color figure can be viewed at wileyonlinelibrary.com]

of T1-hypointensity, each lesion was assigned a T1-contrast ratio value [Van Walderveen et al., 1999], calculated as the signal intensity of the lesion divided by the signal intensity of NAWM.

Acute lesions were classified as “resolving” if after 6 months their volume had shrunk by at least 90% and did not enlarge over this threshold throughout the duration of the study. Acute lesions were classified as “persisting” if their volume did not fall under the inclusion criterion (i.e., 0.3 cm³) for the duration of the study. To follow FLAIR hyperintensity changes in the acute lesions, a FLAIR-contrast ratio to NAWM was calculated in the same manner as the T1-contrast ratio, but utilizing the FLAIR images instead.

¹H MRSI Post-Processing and Absolute Metabolite Quantification

The ¹H MRSI data were Fourier and Hadamard reconstructed along the spectral and spatial directions and each spectrum was frequency-aligned and phased relative to its NAA peak. To maximize lesion inclusion within the ¹H MRSI voxel(s), that is, the region-of-interest (ROI), a procedure known as “voxel shifting” [Barker et al., 2010; Bracewell, 1978] was performed for each lesion, as shown in Figure 1D. Next, the relative levels of the $i = \text{NAA, Cr, Cho}$, mI metabolite in the $j = 1 \dots 480$ voxel were obtained from their peak area, S_{ij} , using the SITools-FITT spectral modeling package [Soher et al., 1998], as shown in Figures 1F–G and 3B. For lesions spanning multiple

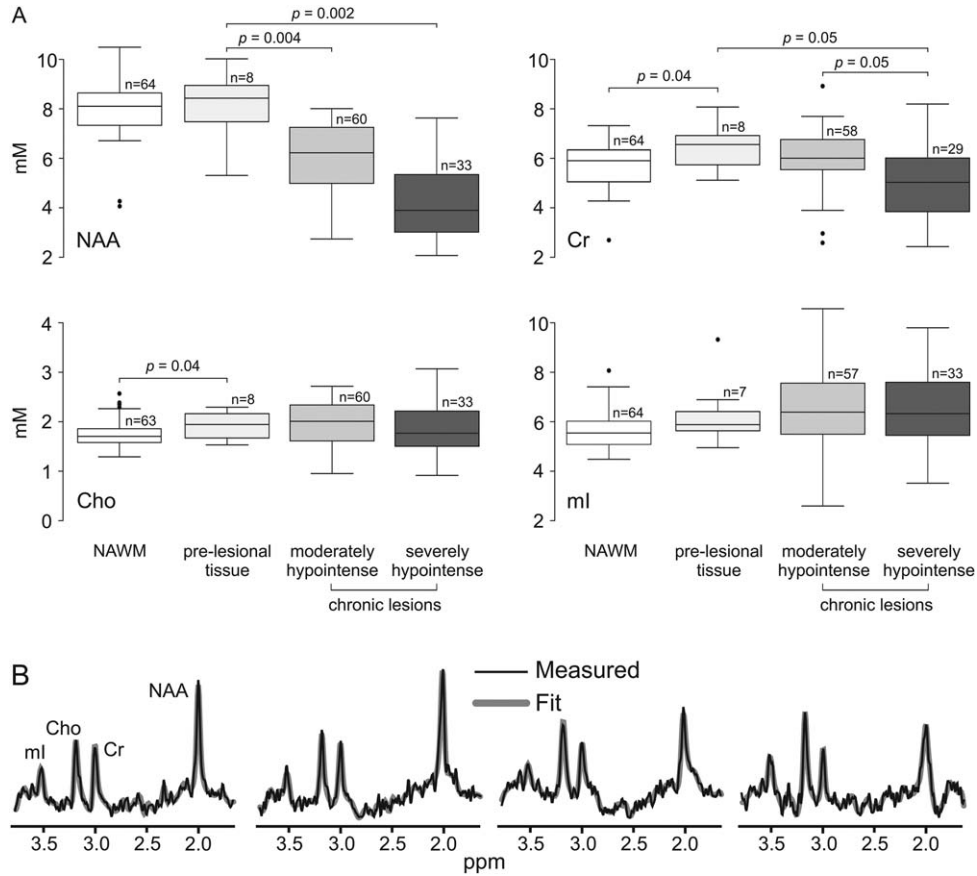


Figure 3.

Metabolite concentrations in NAWM, pre-lesional tissue, and lesions. (A) Boxplots of metabolite concentrations in normal-appearing white matter (NAWM) (white), pre-lesional tissue (beige), moderately hypointense (light gray), and severely hypointense (dark gray) lesions. Indicated are the statistically significant differences obtained from the mixed model analysis of covariance comparing NAWM to pre-lesional tissue; pre-lesional

tissue to moderately and severely hypointense lesions; and moderately to severely hypointense lesions. Note that there was also a statistical trend for lower NAA in severely hypointense versus moderately hypointense lesions. (B) Example spectra from each tissue type (black) shown with their fitted model functions (gray). Left to right: NAWM, pre-lesional tissue, moderately hypointense, and severely hypointense lesion.

voxels, an average S_{ij} was used. The values were normalized for intra-voxel CSF fraction (f_{CSF}) using: $S_{ij}/(1-f_{CSF})$. The corrected values were scaled into absolute amounts, Q_{ij} , relative to a 2 L water-based “Braino” phantom (GE Medical Systems, Milwaukee, WI) with NAA, Cr, Cho, and ml concentrations, C_i^{vitro} , of 12.5, 10.0, 3.0, and 7.5 mmol/L (millimolar, mM):

$$Q_{ij} = C_i^{vitro} \cdot \frac{S_{ij}}{S_{ijR}} \cdot \frac{V_j^{ref}}{V_R^{ref}} \cdot \Lambda_i \left(\frac{\text{millimoles}}{\text{liter}} \right) \quad (1)$$

where S_{ijR} is the sphere’s voxels’ metabolite signal, V_j^{ref} and V_R^{ref} the voltages required for a non-selective 1 ms 180° inversion pulse, and Λ_i a factor accounting for relaxation times differences between each metabolite *in vivo* (T_1^{vivo} , T_2^{vivo}) and in the phantom (T_1^{vitro} , T_2^{vitro}):

$$\Lambda_i = \frac{e^{-TE/T_2^{vitro}}}{e^{-TE/T_2^{vivo}}} \cdot \frac{1 - e^{-TR/T_1^{vitro}}}{1 - e^{-TR/T_1^{vivo}}} \quad (2)$$

The following T_1^{vivo} values were used for NAA, Cr, Cho, and ml: 1,360, 1,300, 1,145, and 1,170 ms [Traber et al., 2004]. Even though no differences were found in T_2^{vivo} of NAA, Cr, and Cho in lesions compared with MS NAWM [Kirov et al., 2010; Van Walderveen et al., 1999], to maximize precision, tissue-specific literature values were used: 296, 163, 199 ms for hypointense lesions, and 298, 162, 222 ms for NAWM and pre-lesional tissue [Kirov et al., 2010]. Since T_2^{vivo} of ml in MS tissue is unknown, 200 ms [Ganji et al., 2012; Posse et al., 2007] was used for all ROIs. The corresponding metabolite relaxation values in the phantom were $T_1^{vitro} = 605, 336, 235, 319$ ms and $T_2^{vitro} = 483, 288, 200, 233$ ms.

¹H MRSI Quality Control

The use of small voxels necessitates strict criteria for spectral quality control. Toward this end, we excluded all voxels comprising more than 30% CSF. Next, we rejected spectra with linewidths under 4 Hz and over 13 Hz [Ebel et al., 2001; Kreis, 2004; Maudsley et al., 2010] and with Cramer-Rao lower bounds of over 20% [Kreis, 2004]. As a last step, visual quality control of each remaining spectrum and its fitting procedure was performed.

Partial Volume Considerations

Accounting for partial volume is critical in longitudinal studies and when examining tissue below the ¹H MRS resolution. In addition to the first inclusion criterion of voxel lesion content >40%, voxels with >30% CSF or >30% GM were excluded. In the follow-up among individual lesions, modulations of CSF and GM partial volume were minimized not to exceed 30% each. For NAMW, only voxels with >97% NAWM, <3% CSF and no GM content were used (these thresholds ensured quantification reproducibility similar to that in global WM of healthy controls [Tal et al., 2012], that is, 9%–15% range for intra- and inter-subject coefficients of variation). All thresholds were applied automatically, with the results undergoing visual inspection. Finally, correction for variable amount of lesion volume within the ¹H MRSI ROI was integrated in all statistical analyses listed next.

Statistical Analysis

Mixed model analysis of covariance was performed to compare NAWM to pre-lesional tissue, pre-lesional tissue to lesions (as a single group, and to the two subgroups, moderately and severely hypointense) and moderately hypointense to severely hypointense lesions in terms of the average level of each metabolite over the entire study period, while accounting for the lack of statistical independence among results derived for the same subject.

Random coefficients regression (RCR) was used to assess changes over time. In NAWM, for each metabolite the dependent variable was the vector of metabolite concentrations from all available timepoints for all subjects. The model included elapsed time from baseline as a fixed numeric factor. To account for variation among subjects at baseline, the intercept was modeled as random, thereby assuming the baseline concentrations to represent a random sample from the population of all patients. To account for statistical dependencies among observations derived for the same patient, an autoregressive covariance structure was modeled thereby assuming observations to be correlated only when acquired from the same patient with the strength of correlation between observations inversely dependent on the elapsed time between them (i.e., measures are more strongly correlated when taken closer together in time). Data were therefore assumed

correlated when obtained from the same patient and independent when obtained from different patients. In lesions, RCR was used to model the temporal change in each metric (metabolite concentration, T1-contrast ratio, lesion size) as a function of elapsed time from initial scan and lesion type. The use of RCR permits a separate linear model to be fit to the data from each lesion and to characterize the change among all lesions of a given type on the basis of an aggregate model, that is, a single line describing the average change in the particular metric among all lesions of the given type. To account for statistical dependencies among data derived for a single individual, the covariance structure was modeled by assuming observations to be correlated only when acquired from the same lesion. The presented rates (mM/month, T1-contrast ratio/month, and cm³/month) refer to changes over the entire follow-up period.

The RCR analysis not only tested the mean rate of change in T1-contrast ratio, volume and each metabolite in each lesion category, but also estimated the rate of change in these metrics for each individual lesion. Relationships between these lesion-level rates of change were characterized in terms of Pearson correlation coefficients.

Relationships of lesion volume and T1-contrast ratio with the level of each metabolite were characterized using partial Pearson correlations. Because larger lesions tend to have lower T1-contrast ratios, to disentangle the effect of one on the other, the correlations with T1-contrast ratio were adjusted for lesion volume, while the correlations with volume were adjusted for T1-contrast ratio. The statistical significance of each correlation was assessed using mixed model regression in order to account for the lack of statistical independence among results derived for the same lesion (at different times) or for lesions within the same patient. The covariance structure was modeled by assuming results to be independent when derived for lesions within different patients, but correlated when acquired from lesions in the same patient with the correlation strongest if the results were associated with the same lesion.

The utility of ¹H MRS to predict future MRI changes was assessed by the Pearson correlation for the association of the rate of change in T1-contrast ratio and volume with baseline metabolite levels.

SAS 9.0 software was used in all calculations. Statistical significance was defined as $P \leq 0.05$ (2-sided), and statistical trends as $0.05 < P \leq 0.07$ (2-sided).

RESULTS

Eight patients did not have lesions which satisfied the minimal volume requirement of 0.3 cm³. The remaining 10 had 21 lesions that passed that threshold. These patients' demographic and clinical data are shown in Table I. There were 64 ¹H MRSI datasets: 7 timepoints in 4 patients and 6 in the remainder. The average scan interval was 7 months. The ¹H MRSI quality control excluded 11 entire

TABLE I. Patient information and lesion timeline

Patient ID	Sex	Age	Disease duration	Baseline			Lesion status over follow-up								
				EDSS	Meds	Lesion ID	Lesion location*	Baseline	6 months	12	18	24	30	36	
1	M	38	2	2.0	GA	1	CC splenium	Pre-lesional	Acute, Gd-		Chronic, MH				
2	F	27	12	1.0	IFN-β1b	2	SCR				Chronic, MH				
3	M	38	15	0.0	IFN-β1a	3	PCR				Chronic, MH				
4	M	30	17	0.0	GA	4	STG WM				Chronic, MH				
5	M	33	24	1.0	IFN-β1a	5	CC splenium	Pre-lesional	Acute, Gd**		Chronic, MH				
6	F	21	28	1.5	-	6	CC body				Chronic, SH				
						7	PCR				Chronic, MH				
						8	SLF				Chronic, SH				
						9	MTG WM				Chronic, SH				
						10	MTG WM				Chronic, SH				
						11	PTR				Chronic, SH				
7	F	32	32	1.0	IFN-β1b	12	O1-WM				Chronic, SH				
						13	PTR				Chronic, MH				
						14	AnG-WM				Chronic, MH				
						15	PTR	Pre-lesional	Acute, Gd-		Chronic, MH				
8	F	26	49	3.0	GA	16	CC body	Pre-lesional	Acute, Gd+		Resolved				
						17	PCR	Pre-lesional	Acute, Gd+		Resolved				
9	F	31	62	2.0	IFN-β1a	18	PCR	Pre-lesional	Acute, Gd+		Chronic, MH				
						19	PTR				Chronic, MH				
						20	SLF				Chronic, MH				
10	M	38	75	1.0	IFN-β1a	21	SCR		Pre-lesional		Acute, Gd+			Resolved	

Left: Patient demographics and clinical information at baseline, sorted by disease duration (months). GA, glatiramer acetate; IFN-β1b, interferon-β1b; IFN-β1a, interferon-β1a.

Right: Timeline of lesion status at each semiannual scan. Gd⁻, noncontrast-enhancing lesion; Gd⁺, contrast-enhancing lesion; MH, moderately hypointense lesion; SH, severely hypointense lesion.

*Lesion location reported based on DTI atlas parcellations [Oishi et al., 2011]: AnG-WM, angular gyrus white matter; CC, corpus callosum; MTG WM, middle temporal gyrus white matter; O1-WM, superior occipital gyrus white matter; PCR, posterior corona radiata; PTR, posterior thalamic radiation; SCR, superior corona radiata; SLF, superior longitudinal fasciculus; STG WM, superior temporal gyrus white matter.

**Enhancement status unknown.

TABLE II. The metabolic concentrations (average ± standard deviation) in millimolar (mM) in each WM tissue type

		Concentration (mM)			
		NAA	Cr	Cho	mI
NAWM		7.9 ± 1.1	5.8 ± 0.8	1.8 ± 0.3	5.7 ± 0.8
Pre-lesional tissue		8.1 ± 1.4	6.5 ± 1.0	2.0 ± 0.3	6.4 ± 1.4
Chronic lesions	Moderately T1-hypointense	5.8 ± 1.5	6.0 ± 1.3	2.0 ± 0.4	6.7 ± 1.7
	Severely T1-hypointense	4.2 ± 1.5	5.0 ± 1.4	1.9 ± 0.5	6.6 ± 1.7

Bold font indicates statistically different concentrations compared with pre-lesional tissue. Not indicated are the results from the concentration comparisons between the moderately and severely T1-hypointense lesions. They showed lower Cr and a trend for lower NAA in the latter. *P* values are listed in the text.

data points and 10 individual metabolite values; 3 data points failed the minimal voxel content requirement either due to being outside the VOI or being split between two of the six ¹H MRSI slices. A total of 116 measurements of pre-lesional tissue (*n* = 8) and lesions (*n* = 108) remained and were used for the statistical analyses. Seventy-seven ¹H MRSI ROIs comprised of 1 voxel, thirty-three of 2, and four had 3 voxels. The median lesion, CSF, and GM fraction within the ¹H MRSI ROI were 57% (range 40%–85%), 0% (0%–29%), and 0% (0%–27%). The corresponding medians of the variations within individual lesions over the follow-up were 21% (5%–40%), 4% (0%–28%), and 8% (2%–24%). The median lesion volume was 0.9 cm³ (0.3–2.5 cm³).

Fifteen lesions were classified as chronic and six as acute. All were T1-hypointense (none met the definition of T1-isointensity). Contrast enhancement was observed in three of the acute lesions and in none of the chronic ones. Of the 15 chronic lesions, 6 were severely hypointense and 9 moderately hypointense. Changes in tissue and lesion classifications over time are shown in Table I. No transitions between hypointensity categories occurred in the chronic lesions. Half of the six acute lesions resolved and half persisted as chronic. All of the latter were moderately hypointense and remained so for the study duration, except for one lesion which converted to severely hypointense at the last timepoint.

The NAWM data, obtained from the 10 patients in Table I, passed the partial volume threshold and ¹H MRSI quality control requirements in all 64 datasets. There were 20 ± 10 (mean ± standard deviation) NAWM voxels per subject, with a median WM fraction of 99% (97%–100%).

Metabolic Differences Between NAWM and Pre-Lesional Tissue

The metabolic concentrations in NAWM and pre-lesional tissue are compiled in Table II, and their distributions are shown in Figure 3A. There were no statistically significant differences between the two tissue types in NAA and mI (*P* > 0.2), while Cr and Cho were higher in pre-lesional tissue (both *P* = 0.04). Example spectra are shown in Figure 3B.

Metabolic Differences Between Pre-Lesional Tissue and Chronic Lesions

Both moderately and severely hypointense lesions had lower NAA than pre-lesional tissue (*P* = 0.004 and *P* = 0.002, respectively). Severely hypointense lesions had lower Cr compared with pre-lesional tissue (*P* = 0.05). These results are shown in Table II and Figure 3A, with example spectra from each lesion type shown in Figure 3B.

Metabolic Differences Between Moderately and Severely Hypointense Lesions

Moderately and severely hypointense lesions differed only in Cr, which was higher in the former (*P* = 0.05), as shown in Figure 3A. There was a statistical trend of lower NAA in the severely versus moderately hypointense lesions (*P* = 0.06).

Serial Changes in NAWM

The baseline NAWM concentrations of NAA, Cr, Cho and mI: 7.5 ± 1.4, 5.4 ± 0.8, 1.6 ± 0.2, and 5.6 ± 0.7 mM did not show statistically significant rates of change over the course of the study. There was, however, a statistical trend for increasing Cho (0.004 mM/month, *P* = 0.07).

Serial Changes in Acute Lesions

After the appearance of a resolving acute lesion, statistically significant rates of change were found for increasing NAA (0.1 mM/month, *P* = 0.01) and increasing T1-contrast ratio (0.004/month, *P* = 0.01), as shown in Figure 4A,B. The temporal behavior of the other metabolites is shown in Figure 4C, and serial images and spectra from one lesion are shown in Figure 4D.

After the appearance of a persisting acute lesion, there was a statistically significant rate of decreasing T1-contrast ratio (−0.002/month, *P* = 0.01). This is shown in Figure 5, along with the temporal behavior of NAA and example serial spectra from one lesion.

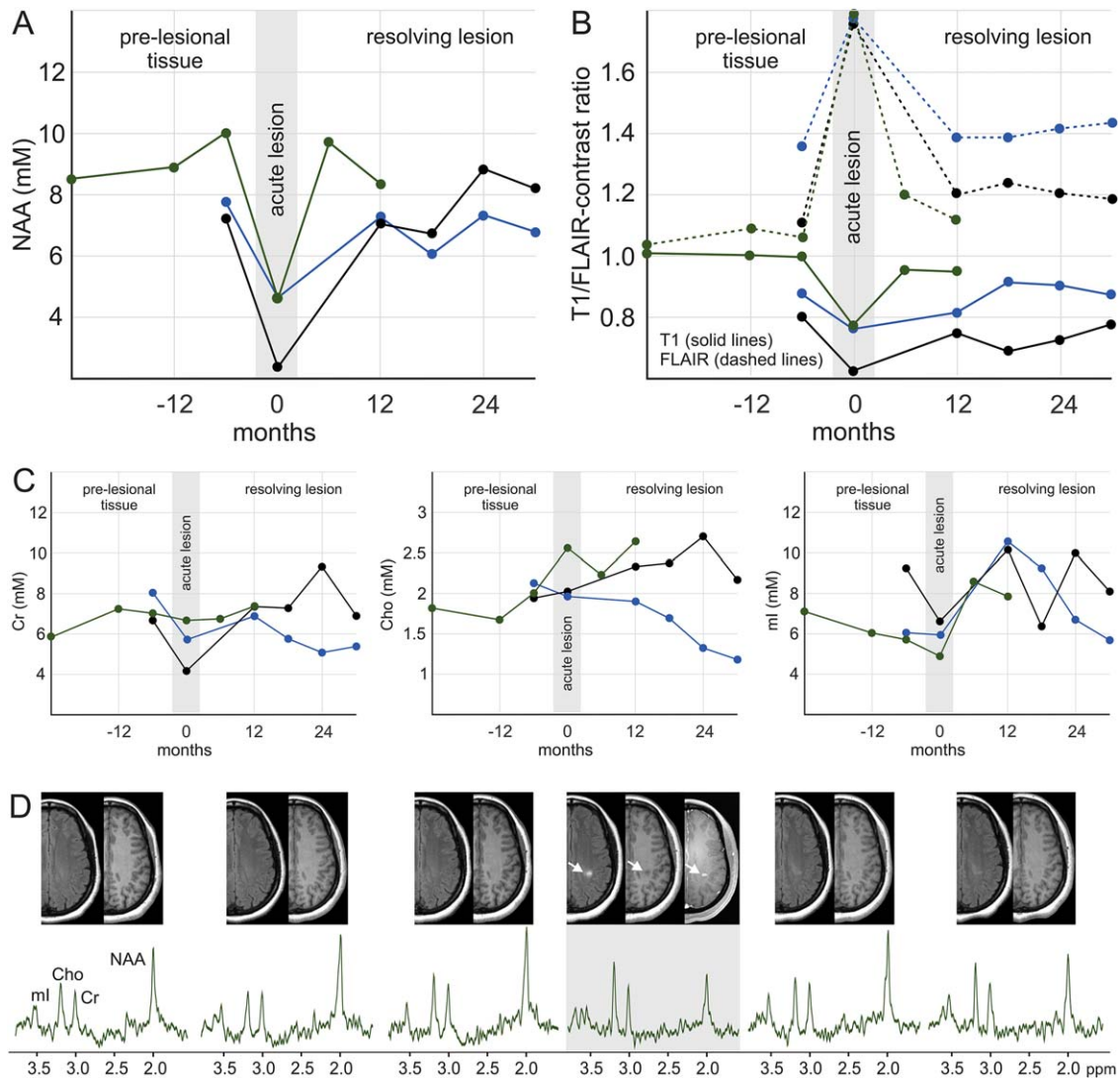


Figure 4.

¹H MRSI and MRI changes in resolving lesions. (A) Changes in NAA concentration and in (B) T1/FLAIR-contrast ratios in the three tissues (green, blue and black lines, corresponding to lesions #20, 16, 17, respectively) undergoing transformation from a pre-lesional state to acute lesion (gray background) to a resolved lesion. (C) The corresponding changes in the concentrations of Cr, Cho, and ml. (D) Top: The FLAIR and MP-

RAGE from which the values of the green lines in (B) were acquired. Note the appearance of the lesion at the fourth time-point, with contrast enhancement shown on the post-gadolinium chelate T1-weighted image. Bottom: The spectra from which the metabolite values of the green lines in (A) and (C) were acquired. Note the similar NAA levels pre- and post-lesion formation. [Color figure can be viewed at wileyonlinelibrary.com]

Serial Changes in Chronic Lesions

In chronic lesions there was a statistically significant rate of change for increasing ml (0.03 mM/month, $P = 0.02$), which was largely driven by its change in moderately hypointense lesions (statistical trend: 0.03 mM/month, $P = 0.06$), as shown in Figure 6A. A statistically significant rate of change was found for decreasing T1-contrast ratio (-0.001 /month, $P = 0.03$), which was also driven by its change in

moderately hypointense lesions (-0.001 /month, $P = 0.04$), as shown in Figure 6B. Serially acquired spectra and images from a moderately hypointense and a severely hypointense chronic lesion are shown in Figure 6C and D. In addition, there was a statistical trend for increasing NAA in moderately hypointense lesions (0.03 mM/month, $P = 0.07$). For each lesion category, the mean rate of change in lesion volume among the lesions was not statistically significant,

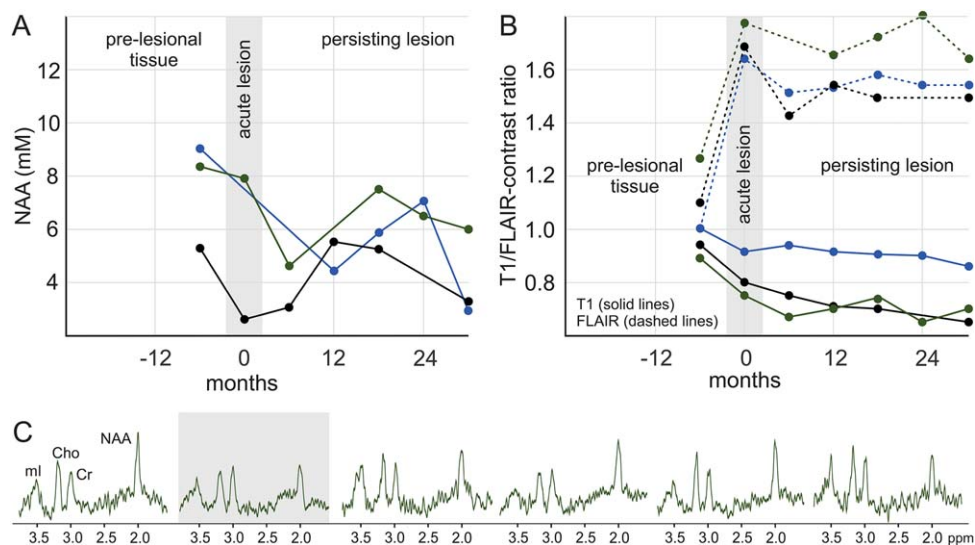


Figure 5.

¹H MRSI and MRI changes in persisting lesions. (A) Changes in NAA concentration and in (B) T1/FLAIR-contrast ratios in the three tissues (green, blue, and black lines, corresponding to lesions #6, 2, 15, respectively) undergoing transformation from a pre-lesional state to acute lesion (gray background) to a persisting lesion. (C) The spectra corresponding to the time course for the green lines in (A) and (B). [Color figure can be viewed at wileyonlinelibrary.com]

although there was a statistical trend for volume increase in the severely hypointense lesions ($0.01 \text{ cm}^3/\text{month}$, $P = 0.06$).

Correlations Between Metabolism and MRI

The relationships between metabolite concentrations and T1-contrast ratio and between metabolite concentrations and lesion volume are shown in Figure 7. Of these, the only statistically significant correlation was an inversely proportional relationship of NAA with lesion volume ($r = -0.3$, $P = 0.04$), while there was a statistical trend of an inversely proportional relationship of Cr also with lesion volume ($r = -0.3$, $P = 0.06$).

There were statistically significant correlations between the lesion-level rates of change of NAA and of T1-contrast ratio, and of mI and T1-contrast ratio in acute lesions ($r = 0.9$, $P = 0.02$; $r = 1.0$, $P = 0.001$). Lesion-level rate of change in lesion volume correlated with lesion-level rate of change in Cho within moderately hypointense lesions ($r = 0.8$, $P = 0.01$).

There were no statistically significant correlations between baseline metabolite concentrations and rates of change in lesion volume (all $P > 0.3$) and in T1-contrast ratio (all $P > 0.5$).

DISCUSSION

Study Approach—Methodology

Lesions identified on T1- and T2-weighted MRI are the most widely used imaging metric in the clinical management

of MS: diagnosis is based on lesion evolution in space and time, long term prognosis is well predicted by the magnitude of lesion load at diagnosis [Poloni et al., 2011], and treatment decisions are guided by the rate of lesion accumulation. The standard in imaging outcomes for clinical trials is also lesion monitoring, through changes in number, volume, enhancement and T1-hypointensity [Cohen et al., 2012; Miller, 2004].

Unfortunately, the metabolic processes underlying these monitoring criteria and clinical trial end points are still not fully understood. This is in part due to the spatial resolution of ¹H MRS, which results in partial volume contamination of the lesion from normal-appearing tissue and CSF. To circumvent this problem, metabolic ratios have been used, but they account only for CSF contamination. A second approach has been to focus exclusively on lesions large enough to fill the entire voxel [Davie et al., 1994, 1997; He et al., 2005; Simone et al., 2001]. These, however, are uncharacteristic of the disease. Moreover, the vast majority of past studies have used single voxels, which require lesion selection, voxel sizing and voxel placement to be made during the scan, resulting in suboptimal, time-constrained lesion selection and partial volume control. In contrast, ¹H MRSI allows retrospective lesion selection, and voxel lesion content optimization through voxel shifting.

In this study, all lesions conformed to a minimum size requirement and to thresholds of CSF and GM. This partial volume control optimizes the precision and accuracy of the experiment: the former by decreasing the variations caused by non-lesional volume, and the latter by maximizing voxel lesion content. Next, because lesions tend to be located

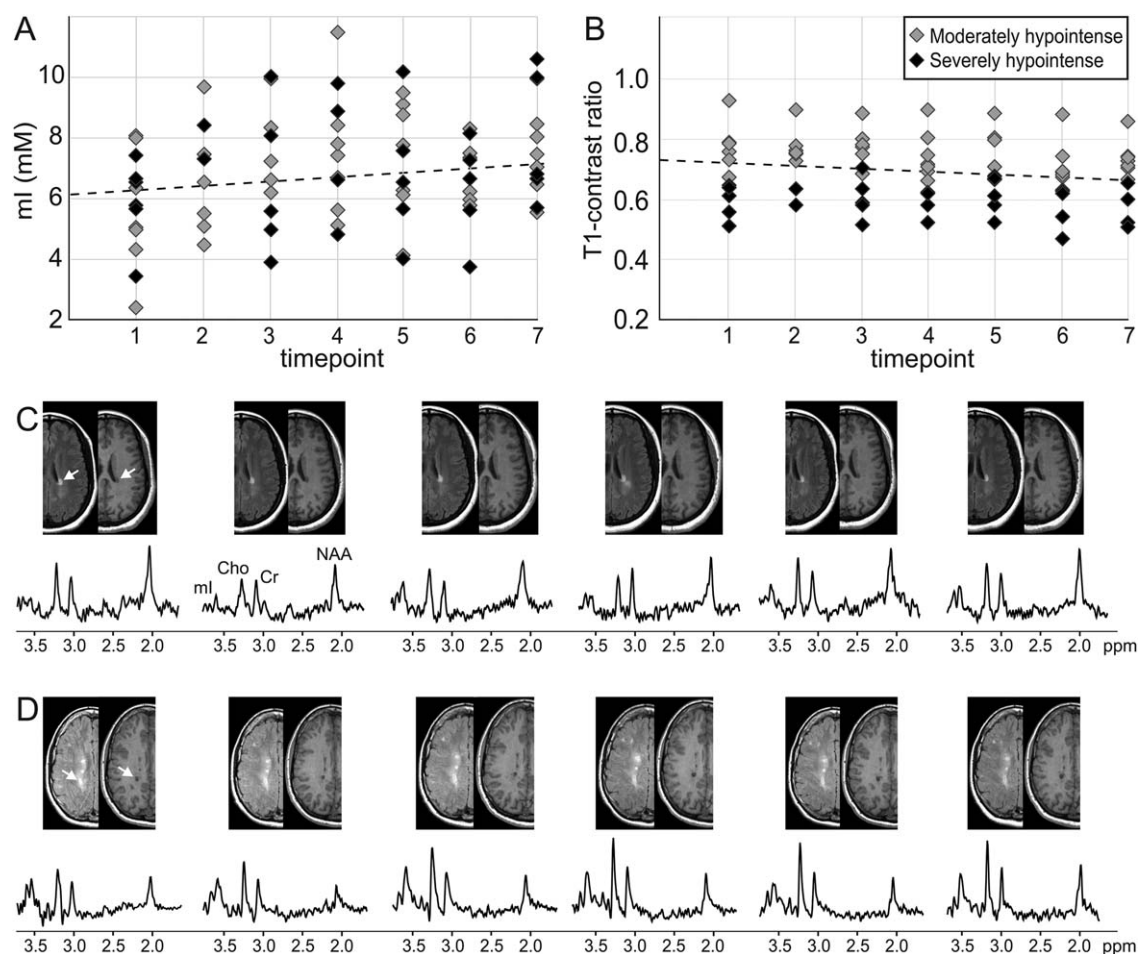


Figure 6.

¹H MRSI and MRI changes in chronic lesions. (A) Changes in ml concentration and (B) T1-contrast ratio among all chronic lesions, with dotted lines indicating their rates of change as statistically significant. Moderately (gray diamonds) and severely (black diamonds) hypointense lesions are individually indicated

to highlight that these findings are largely driven by changes in moderately hypointense lesions. (C) Serial FLAIR, MP-RAGE and spectra from a moderately hypointense chronic lesion (#18 in Table I). (D) Serial FLAIR, MP-RAGE and spectra from a severely hypointense chronic lesion (#7 in Table I).

periventricularly (c.f., Figs. 1 and 2), voxel CSF content was additionally controlled: we excluded voxels with more than 30% CSF and scaled the signal of the remaining voxels proportionally for any remaining amount. Finally, all statistical analyses took into account the amount of voxel lesion content. Overall, therefore, a major methodological advantage of the current study was the level of partial volume control.

Another factor limiting our understanding of lesion metabolism is the use of metabolic ratios, which do not reveal whether changes are due to the numerator or denominator. The absolute quantification employed here maximizes the available ¹H MRS specificity to neuronal and glial injury, and avoids scenarios in which the numerator and denominator of metabolic ratios change in unison, decreasing the observed effect sizes [Davies et al., 1995].

Study Approach—Clinical

These methodological advantages facilitate reliable estimation of metabolic concentrations in individual, sub-1 cm³ lesions found in early, mildly disabled patients. The cohort’s homogeneity in terms of disability and disease duration is important in light of the known histopathological and MRI differences in lesion evolution between early and late MS [Filippi et al., 2012]. The 3D ¹H MRSI coverage of the most prominent lesion predilection sites (periventricular, subcortical forebrain WM [Lassmann, 2008]), allowed for a wide study scope with the following novel aspects: (i) follow-up of pre-lesional tissue through the acute stage and conversion to resolved or chronic lesions; (ii) follow-up of individual chronic lesions; (iii) relating the metabolic data

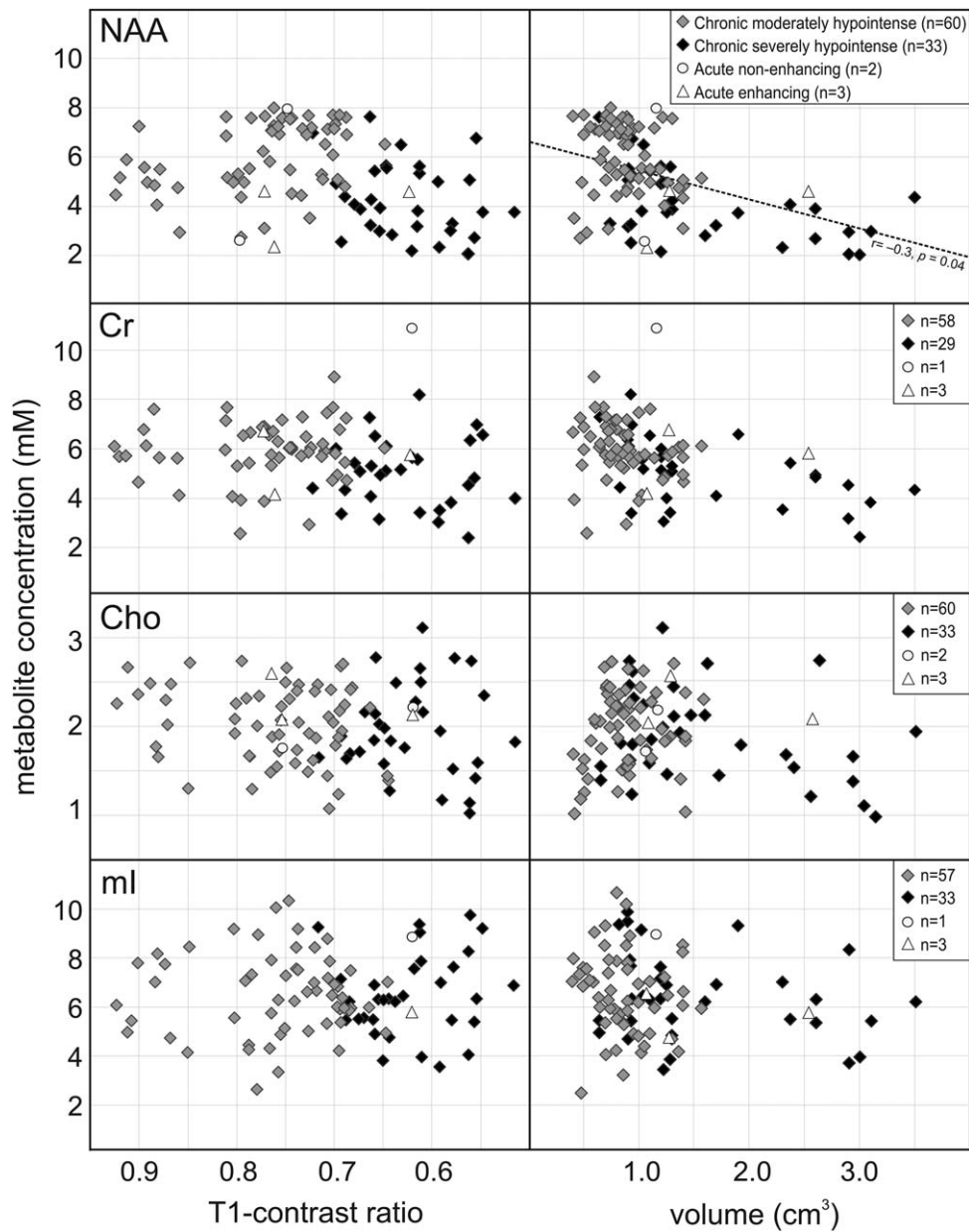


Figure 7.

Cross-sectional relationships between lesion ¹H MRS and MRI. Lesion metabolite concentrations (in millimolar, mM) as a function of lesion T1-contrast ratio (left), and volume (right). The statistical analyses, adjusted for the relationship between T1-contrast ratio and lesion volume, showed statistically significant correlation only between NAA and lesion volume (dotted line), with a statistical trend for a correlation between Cr and lesion volume. All lesions are shown,

categorized according to the legend, with sample sizes indicated for each metabolite (totals differ due to data points excluded in the quality control). Note that NAA levels decrease as a function of T1-contrast ratio only within severely hypointense lesions, but that this relationship is mediated by lesion volume. Also note the cut-off at approximately 1.5 cm³ over which lesions exhibit very low NAA within a very narrow range of values, indicating terminal axonal injury.

to quantitative measurements of both accepted MRI metrics of lesion severity: hypointensity and volume. The results shed light on lesion pathogenesis and pathophysiology, and

inform about the metabolic correlates of lesion appearance on conventional MRI, as encountered in everyday clinical practice.

Normal-Appearing White Matter

Depending on whether it converted to a lesion over the follow-up, WM was defined as NAWM or as pre-lesional tissue. The results revealed differences in metabolite levels between these two entities. Levels of Cr and Cho were higher in pre-lesional tissue, suggesting that lesion-related glial pathology inflicts NAWM prior to its conversion. These findings are in line with the two previous studies of pre-lesional tissue [Narayana et al., 1998; Tartaglia et al., 2002], which also found evidence of higher Cho compared with NAWM. As hypothesized also by those investigators, the most likely interpretation is that the elevated Cho signal reflects inflammation-induced myelin pathology present prior to a breakdown in the blood–brain barrier.

It is outside the scope of this project to compare the NAWM results to healthy WM. The reader is referred to two studies from our group [Kirov et al., 2009, 2013] in patients which include the 18 initially enrolled for the current study. The results support the literature consensus that NAWM in MS has abnormal metabolism [Filippi and Rocca, 2011; Miller et al., 2003].

Pre-Lesional Tissue

Concentrations of Cr, Cho, and mI in pre-lesional tissue were not different from those in chronic lesions, suggesting that the processes represented by these metabolites are present at lesion-like levels prior to lesion formation. The most likely interpretation of this finding is that the combination of inflammation and gliosis in pre-lesional tissue is similar to chronic lesions'. The observation that all three glial markers are involved is suggestive of gliosis, a well-known histopathological feature of MS NAWM [Allen and McKeown, 1979]. Specifically, glia have higher concentrations of Cr and Cho than neurons [Urenjak et al., 1993] and the mI signal is thought to be specific to astrocytes [Brand et al., 1993]. Additionally, in MS NAWM phosphorus MRS has shown that high Cr levels are associated with gliosis rather than energy imbalance [Hattingen et al., 2011], and a combined ¹H MRS-histopathology study related Cho with gliosis [Bitsch et al., 1999].

In contrast to the glial markers, NAA in pre-lesional tissue was statistically higher compared with both moderately and severely hypointense lesions. Since the NAA signal is a surrogate marker for neuronal health [Moffett et al., 2007], this indicates that established lesions sustain previously absent axonal injury. The finding of higher Cr in pre-lesional tissue compared with severely hypointense lesions is likely related to the large NAA deficit in the latter subgroup, indicative of permanent axonal damage, which, in turn, leads to lower energy demand.

Acute Lesions

The appearance of an acute lesion is accompanied by a drop of NAA, as shown in Figures 4A and 5A. A key

finding of the current study was that NAA levels showed a statistically significant recovery in the months following the appearance of an acute lesion which concurrently resolved on T2-weighted MRI (Fig. 4A,B). Moreover, as shown in Figure 4B, this recovery correlated with decreasing hypointensity on T1-weighted MRI, indicating that in transient hypointense lesions, retaining isointensity is associated with a normalization of NAA to pre-lesional levels. In persisting lesions, no NAA changes were found, although we note a visual, but non-statistically significant increase following the acute stage (Fig. 5A). Previous serial ¹H MRS studies support the notion of NAA recovery after the acute stage [Davie et al., 1994; Mader et al., 2000; Narayana et al., 1998; Zaaraoui et al., 2010], but none tested it statistically, nor distinguished transient from persistent lesions. Although we are unable to differentiate the contributions of axonal injury and vasogenic edema to the NAA decline (see "Limitations" below), the results here suggest lack of long-lasting damage within acute transient hypointense lesions. This has implications for trials utilizing lesion MRI outcomes, as it substantiates the notion that transient hypointense lesions represent a return to pre-lesional axonal state, and are therefore the preferred outcome also from a metabolic point of view.

Chronic Lesions

Acute lesions that do not resolve after 6 months can be considered chronic [Davie et al., 1997]. To account for the wide range of T1-hypointensity, contrast ratios were calculated and chronic lesions were dichotomized into moderately and severely hypointense. The severely hypointense group had lower Cr and a statistical trend for lower NAA, while no differences or trends were found for Cho and mI. In line with previous ¹H MRS [Brex et al., 2000; He et al., 2005; Van Walderveen et al., 1999] and histopathology [Van Waesberghe et al., 1999; Van Walderveen et al., 1998] studies, these results add to the consensus that very hypointense lesions suffer more neuronal damage than less hypointense ones, and that the underlying cause is low overall cell density.

Our study also reveals, however, that the metabolic dependency on T1-hypointensity is not linear. As shown in Figure 7, NAA decreases as a function of T1-hypointensity only in severely hypointense lesions. Moreover, this relationship was found to be mediated by lesion volume, which was a better predictor of low NAA than T1-hypointensity. Intriguingly, there was a clear divide in NAA concentrations at lesion volume of approximately 1.5 cm³. Larger lesions had concentrations within a very narrow, approximately 2–4.5 mM range, in contrast to the approximately 2–8 mM range of smaller lesions, suggesting terminal axonal injury in the former versus more heterogeneous axonal status in the latter. This finding highlights the importance of taking lesion volume as a covariate in imaging and histopathological studies, especially

since large lesions tend to be very T1-hypointense. Even without considerations of T1-hypointensity, grouping together patients with different proportions of lesion sizes could confound the measurement of NAA and Cr.

The serial data revealed an increase in mI, primarily in moderately hypointense lesions. Since one of the histopathological hallmarks of the MS lesion is astrogliosis, these results likely demonstrate its accumulation over time, especially in less T1-hypointense lesions. While this was the only statistically significant metabolite change, there was also a statistical trend for NAA increase in moderately hypointense lesions. With this caveat, we note that findings of increasing NAA in lesions and NAWM can be attributed to medication [Khan et al., 2008; Narayanan et al., 2001; Wiebenga et al., 2015], and therefore it can be speculated that our results suggest such an effect, but only in moderately hypointense lesions.

Comparisons between metabolic and MRI rates of change in chronic lesions generated only one, yet important finding: a positive correlation between changes in Cho and lesion volume for moderately hypointense lesions. This implies that changes in lesion size are mediated by the level of chronic inflammation. We note that this is in accordance with histopathological findings in the “slowly expanding lesion” type, as put forth by Lassmann, to describe chronic, non-enhancing, growing lesions, containing subtle inflammation only at lesions’ edge [Lassmann, 2008].

From both the serial and cross-sectional results, it is clear that moderately hypointense lesions are more metabolically active than severely hypointense ones. The change seen on conventional MRI in the two groups was also different: the former exhibited decreasing T1-contrast ratio, while the latter a statistical trend for increasing volume. These MRI findings are noteworthy on their own accord, indicating that in chronic lesions, increase in T1-hypointensity precedes enlargement.

LIMITATIONS

Only T1-hypointense lesions fulfilled the inclusion criteria, precluding the study of isointense lesions. This is likely unavoidable given the need for a minimal lesion size requirement, biasing our selection to larger lesions which tend to be more T1-hypointense (as shown in Fig. 7). In addition, the criteria for isointensity was strict, excluding even subtly hypointense lesions.

The 6 month follow-up is more appropriate for monitoring chronic rather than acute lesions, as the latter change on time scale of weeks. On the other hand, we were able to confirm the resolved/persistent status of acute lesions as far ahead as 2 years post-formation, and to relate it to their long-term metabolism. Another caveat related to the results from the acute lesions is that the conclusions are based on a small sample size (3 resolving, 3 persisting lesions), and therefore should be interpreted with caution.

The difficulty in capturing the acute stage within a longitudinal design is reflected throughout the ¹H MRS literature, with previous studies reporting serial data from similar number of acute lesions [Arnold et al., 1992; Davie et al., 1994; Narayana et al., 1998; Zaaraoui et al., 2010]. Encouragingly, however, all results, including ours, are in line with the notion of NAA recovery after the acute stage, with the data here suggesting that this is most apparent in lesions that resolve, rather than in those which persist as chronic. Unfortunately, since none of the cited studies, or ours, corrected for edema in contrast-enhancing lesions, the magnitude of the NAA decline due to vasogenic edema and not neuronal insult, is unknown. In this work, there was an apparent reduction in most metabolite concentrations within the contrast-enhancing lesions (c.f., Fig. 4A and C) which implies potentially underestimated values. Regardless of why NAA declines at lesion formation, however, transient new lesions do not induce long-lasting axonal damage, as inferred from the similar NAA levels in the pre-lesional and resolved state. This is important, since lesions do cause an NAA decline; the question of when that happens is still open, but one possibility is suggested by Figure 5A, which shows that the persisting lesions’ NAA falls below baseline levels approximately two years post-formation.

In order to maintain reasonable statistical power with data from only 21 lesions, statistical tests were conducted without a multiple comparison correction. Consequently, our significant findings may include type I errors (false positives) and should be independently replicated.

Finally, despite compelling evidence for abnormal glutamate in lesions [Srinivasan et al., 2005], our small voxel size represented a trade-off between studying smaller lesions and adequate signal-to-noise ratio to detect glutamate.

CONCLUSION

We describe lesion evolution in early MS from a quantitative ¹H MRS and MRI perspective. The full range of lesion states is studied through cross-sectional and serial analyses of absolute metabolic concentrations and lesion T1-hypointensity and T2-volume. The results reveal the metabolic underpinnings of lesion appearance on conventional imaging, and inform about disease progression within the hallmark pathology of MS.

ACKNOWLEDGMENTS

The authors would like to dedicate this research to the memory of our late colleague, Dr. Joseph Herbert. We are grateful to the research participants and to the study coordinator Nissa N. Perry. Dr. Assaf Tal acknowledges the support of the Monroy-Marks Career Development Fund, the Carolito Stiftung Fund, the Leona M. and Harry B. Helmsley Charitable Trust, the Sylvia Schaefer Alzheimer’s

Research Fund and the historic generosity of the Harold Perlman Family.

REFERENCES

- Allen IV, McKeown SR (1979): A histological, histochemical and biochemical study of the macroscopically normal white matter in multiple sclerosis. *J Neurol Sci* 41:81–91.
- Arnold DL, Matthews PM, Francis GS, O'Connor J, Antel JP (1992): Proton magnetic resonance spectroscopic imaging for metabolic characterization of demyelinating plaques. *Ann Neurol* 31:235–241.
- Ashburner J, Friston K (1997): Multimodal image coregistration and partitioning—a unified framework. *Neuroimage* 6:209–217.
- Barker P, Bizzi A, De Stefano N, Gullapalli RP, Lin DDM (2010): Spectral analysis methods, quantitation, and common artifacts. *Clinical MR Spectroscopy, Techniques and Applications*. Cambridge: Cambridge University Press.
- Bitsch A, Bruhn H, Vougioukas V, Stringaris A, Lassmann H, Frahm J, Bruck W (1999): Inflammatory CNS demyelination: Histopathologic correlation with in vivo quantitative proton MR spectroscopy. *AJNR Am J Neuroradiol* 20:1619–1627.
- Bracewell RN (1978): *The Fourier Transform and Its Applications*. New York: McGraw-Hill.
- Brand A, Richter-Landsberg C, Leibfritz D (1993): Multinuclear NMR studies on the energy metabolism of glial and neuronal cells. *Dev Neurosci* 15:289–298.
- Brex PA, Parker GJ, Leary SM, Molyneux PD, Barker GJ, Davie CA, Thompson AJ, Miller DH (2000): Lesion heterogeneity in multiple sclerosis: A study of the relations between appearances on T1 weighted images, T1 relaxation times, and metabolite concentrations. *J Neurol Neurosurg Psychiatry* 68:627–632.
- Brooker HR, Mareci TH, Mao JT (1987): Selective Fourier transform localization. *Magn Reson Med* 5:417–433.
- Chard DT, Jackson JS, Miller DH, Wheeler-Kingshott CA (2010): Reducing the impact of white matter lesions on automated measures of brain gray and white matter volumes. *J Magn Reson Imaging* 32:223–228.
- Cohen JA, Reingold SC, Polman CH, Wolinsky JS, International Advisory Committee on Clinical Trials in Multiple Sclerosis (2012): Disability outcome measures in multiple sclerosis clinical trials: Current status and future prospects. *Lancet Neurol* 11:467–476.
- Davie CA, Hawkins CP, Barker GJ, Brennan A, Tofts PS, Miller DH, McDonald WI (1994): Serial proton magnetic resonance spectroscopy in acute multiple sclerosis lesions. *Brain* 117:49–58.
- Davie CA, Barker GJ, Thompson AJ, Tofts PS, McDonald WI, Miller DH (1997): 1H magnetic resonance spectroscopy of chronic cerebral white matter lesions and normal appearing white matter in multiple sclerosis. *J Neurol Neurosurg Psychiatry* 63:736–742.
- Davies SE, Newcombe J, Williams SR, McDonald WI, Clark JB (1995): High resolution proton NMR spectroscopy of multiple sclerosis lesions. *J Neurochem* 64:742–748.
- Ebel A, Soher BJ, Maudsley AA (2001): Assessment of 3D proton MR echo-planar spectroscopic imaging using automated spectral analysis. *Magn Reson Med* 46:1072–1078.
- Filippi M, Rocca MA (2011): MR imaging of multiple sclerosis. *Radiology* 259:659–681.
- Filippi M, Rocca MA, De Stefano N, Enzinger C, Fisher E, Horsfield MA, Inglesse M, Pelletier D, Comi G (2011): Magnetic resonance techniques in multiple sclerosis: The present and the future. *Arch Neurol* 68:1514–1520.
- Filippi M, Rocca MA, Barkhof F, Bruck W, Chen JT, Comi G, Deluca G, De Stefano N, Erickson BJ, Evangelou N, Fazekas F, Geurts JJ, Lucchinetti C, Miller DH, Pelletier D, Popescu BF, Lassmann H (2012): Association between pathological and MRI findings in multiple sclerosis. *Lancet Neurol* 11:349–360.
- Frohman EM, Racke MK, Raine CS (2006): Multiple sclerosis—the plaque and its pathogenesis. *N Engl J Med* 354:942–955.
- Ganji SK, Banerjee A, Patel AM, Zhao YD, Dimitrov IE, Browning JD, Brown ES, Maher EA, Choi C (2012): T2 measurement of J-coupled metabolites in the human brain at 3T. *NMR Biomed* 25:523–529.
- Goelman G, Liu S, Gonen O (2006a): Reducing voxel bleed in Hadamard-encoded MRI and MRS. *Magn Reson Med* 55:1460–1465.
- Goelman G, Liu S, Hess D, Gonen O (2006b): Optimizing the efficiency of high-field multivoxel spectroscopic imaging by multiplexing in space and time. *Magn Reson Med* 56:34–40.
- Hattingen E, Magerkurth J, Pilatus U, Hubers A, Wahl M, Ziemann U (2011): Combined (1)H and (31)P spectroscopy provides new insights into the pathobiochemistry of brain damage in multiple sclerosis. *NMR Biomed* 24:536–546.
- He J, Inglesse M, Li BS, Babb JS, Grossman RI, Gonen O (2005): Relapsing-remitting multiple sclerosis: Metabolic abnormality in nonenhancing lesions and normal-appearing white matter at MR imaging: Initial experience. *Radiology* 234:211–217.
- Hu J, Javaid T, Arias-Mendoza F, Liu Z, McNamara R, Brown TR (1995): A fast, reliable, automatic shimming procedure using 1H chemical-shift-imaging spectroscopy. *J Magn Reson B* 108:213–219.
- Khan O, Shen Y, Bao F, Caon C, Tselis A, Latif Z, Zak I (2008): Long-term study of brain 1H-MRS study in multiple sclerosis: Effect of glatiramer acetate therapy on axonal metabolic function and feasibility of long-Term H-MRS monitoring in multiple sclerosis. *J Neuroimaging* 18:314–319.
- Kirov II, Patil V, Babb JS, Rusinek H, Herbert J, Gonen O (2009): MR spectroscopy indicates diffuse multiple sclerosis activity during remission. *J Neurol Neurosurg Psychiatry* 80:1330–1336.
- Kirov II, Liu S, Fleysher R, Fleysher L, Babb JS, Herbert J, Gonen O (2010): Brain metabolite proton T2 mapping at 3.0 T in relapsing-remitting multiple sclerosis. *Radiology* 254:858–866.
- Kirov II, Tal A, Babb JS, Herbert J, Gonen O (2013): Serial proton MR spectroscopy of gray and white matter in relapsing-remitting MS. *Neurology* 80:39–46.
- Kreis R (2004): Issues of spectral quality in clinical 1H-magnetic resonance spectroscopy and a gallery of artifacts. *NMR Biomed* 17:361–381.
- Lassmann H (2008): The pathologic substrate of magnetic resonance alterations in multiple sclerosis. *Neuroimaging Clin N Am* 18:563–576.
- Lublin FD, Reingold SC, Cohen JA, Cutter GR, Sorensen PS, Thompson AJ, Wolinsky JS, Balcer LJ, Banwell B, Barkhof F, Bebo B, Jr., Calabresi PA, Clanet M, Comi G, Fox RJ, Freedman MS, Goodman AD, Inglesse M, Kappos L, Kieseier BC, Lincoln JA, Lubetzki C, Miller AE, Montalban X, O'Connor PW, Petkau J, Pozzilli C, Rudick RA, Sormani MP, Stuve O, Waubant E, Polman CH (2014): Defining the clinical course of multiple sclerosis: The 2013 revisions. *Neurology* 83:278–286.
- Mader I, Roser W, Kappos L, Hagberg G, Seelig J, Radue EW, Steinbrich W (2000): Serial proton MR spectroscopy of contrast-enhancing multiple sclerosis plaques: Absolute

- metabolic values over 2 years during a clinical pharmacological study. *Am J Neuroradiol* 21:1220–1227.
- Mareci T, Brooker H (1991): Essential considerations for spectral localization using indirect gradient encoding of spatial information. *J Magn Reson* 92:229–246.
- Maudsley AA, Domenig C, Sheriff S (2010): Reproducibility of serial whole-brain MR spectroscopic imaging. *NMR Biomed* 23:251–256.
- Miller DH (2004): Biomarkers and surrogate outcomes in neurodegenerative disease: Lessons from multiple sclerosis. *NeuroRx* 1:284–294.
- Miller DH, Thompson AJ, Filippi M (2003): Magnetic resonance studies of abnormalities in the normal appearing white matter and grey matter in multiple sclerosis. *J Neurol* 250:1407–1419.
- Moffett JR, Ross B, Arun P, Madhavarao CN, Namboodiri AM (2007): N-Acetylaspartate in the CNS: From neurodiagnostics to neurobiology. *Prog Neurobiol* 81:89–131.
- Narayana PA, Doyle TJ, Lai D, Wolinsky JS (1998): Serial proton magnetic resonance spectroscopic imaging, contrast-enhanced magnetic resonance imaging, and quantitative lesion volumetry in multiple sclerosis. *Ann Neurol* 43:56–71.
- Narayanan S, De Stefano N, Francis GS, Arnaoutelis R, Caramanos Z, Collins DL, Pelletier D, Arnason BGW, Antel JP, Arnold DL (2001): Axonal metabolic recovery in multiple sclerosis patients treated with interferon beta-1b. *J Neurol* 248: 979–986.
- Oishi K, Faria AV, van Zijl PCM, Mori S (2011): *MRI Atlas of Human White Matter*. 2nd edition, Elsevier, ISBN: 9780123820815.
- Poloni G, Minagar A, Haacke EM, Zivadinov R (2011): Recent developments in imaging of multiple sclerosis. *Neurologist* 17: 185–204.
- Poser CM, Paty DW, Scheinberg L, McDonald I, Davis FA, Ebers GC, Johnson KP, Sibley WA, Silberberg DH, Tourtelloutte WW (1983): New diagnostic criteria for multiple sclerosis: Guidelines for research protocols. *Ann Neurol* 13:227–231.
- Posse S, Otazo R, Caprihan A, Bustillo J, Chen H, Henry PG, Marjanska M, Gasparovic C, Zuo C, Magnotta V, Mueller B, Mullins P, Renshaw P, Ugurbil K, Lim KO, Alger JR (2007): Proton echo-planar spectroscopic imaging of J-coupled resonances in human brain at 3 and 4 Tesla. *Magn Reson Med* 58: 236–244.
- Rovira A, Alonso J (2013): 1H magnetic resonance spectroscopy in multiple sclerosis and related disorders. *Neuroimaging Clin N Am* 23:459–474.
- Rusinek H, Glodzik L, Mikheev A, Zanotti A, Li Y, De Leon M (2013): Fully automatic segmentation of white matter lesions: Error analysis and validation of a new tool. *Int J Comput Assist Radiol Surg* 8:289–291.
- Sajja BR, Wolinsky JS, Narayana PA (2009): Proton magnetic resonance spectroscopy in multiple sclerosis. *Neuroimaging Clin N Am* 19:45–58.
- Sigmund EE, Vivier PH, Sui D, Lamparello NA, Tantillo K, Mikheev A, Rusinek H, Babb JS, Storey P, Lee VS, Chandarana H (2012): Intravoxel incoherent motion and diffusion-tensor imaging in renal tissue under hydration and furosemide flow challenges. *Radiology* 263:758–769.
- Simone IL, Tortorella C, Federico F, Liguori M, Lucivero V, Giannini P, Carrara D, Bellacosa A, Livrea P (2001): Axonal damage in multiple sclerosis plaques: A combined magnetic resonance imaging and 1H-magnetic resonance spectroscopy study. *J Neurol Sci* 182:143–150.
- Soher BJ, Young K, Govindaraju V, Maudsley AA (1998): Automated spectral analysis III: Application to in vivo proton MR spectroscopy and spectroscopic imaging. *Magn Reson Med* 40: 822–831.
- Sormani MP, Bruzzi P (2013): MRI lesions as a surrogate for relapses in multiple sclerosis: A meta-analysis of randomised trials. *Lancet Neurol* 12:669–676.
- Srinivasan R, Sailasuta N, Hurd R, Nelson S, Pelletier D (2005): Evidence of elevated glutamate in multiple sclerosis using magnetic resonance spectroscopy at 3 T. *Brain* 128:1016–1025.
- Tal A, Kirov II, Grossman RI, Gonen O (2012): The role of gray and white matter segmentation in quantitative proton MR spectroscopic imaging. *NMR Biomed* 25:1392–1400.
- Tartaglia MC, Narayanan S, De Stefano N, Arnaoutelis R, Antel SB, Francis SJ, Santos AC, Lapierre Y, Arnold DL (2002): Choline is increased in pre-lesional normal appearing white matter in multiple sclerosis. *J Neurol* 249:1382–1390.
- Traber F, Block W, Lamerichs R, Gieseke J, Schild HH (2004): 1H metabolite relaxation times at 3.0 tesla: Measurements of T1 and T2 values in normal brain and determination of regional differences in transverse relaxation. *J Magn Reson Imaging* 19: 537–545.
- Trapp BD, Bo L, Mork S, Chang A (1999): Pathogenesis of tissue injury in MS lesions. *J Neuroimmunol* 98:49–56.
- Urenjak J, Williams SR, Gadian DG, Noble M (1993): Proton nuclear magnetic resonance spectroscopy unambiguously identifies different neural cell types. *J Neurosci* 13:981–989.
- Van Waesberghe JH, Kamphorst W, De Groot CJ, Van Walderveen MA, Castelijns JA, Ravid R, Lycklama a, Nijeholt GJ, van der Valk P, Polman CH, Thompson AJ, Barkhof F (1999): Axonal loss in multiple sclerosis lesions: Magnetic resonance imaging insights into substrates of disability. *Ann Neurol* 46:747–754.
- Van Walderveen MA, Kamphorst W, Scheltens P, van Waesberghe JH, Ravid R, Valk J, Polman CH, Barkhof F (1998): Histopathologic correlate of hypointense lesions on T1-weighted spin-echo MRI in multiple sclerosis. *Neurology* 50: 1282–1288.
- Van Walderveen MA, Barkhof F, Pouwels PJ, van Schijndel RA, Polman CH, Castelijns JA (1999): Neuronal damage in T1-hypointense multiple sclerosis lesions demonstrated in vivo using proton magnetic resonance spectroscopy. *Ann Neurol* 46:79–87.
- Wiebenga OT, Klauser AM, Schoonheim MM, Nagtegaal GJ, Steenwijk MD, van Rossum JA, Polman CH, Barkhof F, Pouwels PJ, Geurts JJ (2015): Enhanced axonal metabolism during early natalizumab treatment in relapsing-remitting multiple sclerosis. *AJNR Am J Neuroradiol* 36:1116–1123.
- Zaaraoui W, Rico A, Audoin B, Reuter F, Malikova I, Soulier E, Viout P, Le Fur Y, Confort-Gouny S, Cozzone PJ, Pelletier J, Ranjeva JP (2010): Unfolding the long-term pathophysiological processes following an acute inflammatory demyelinating lesion of multiple sclerosis. *Magn Reson Imaging* 28:477–486.